
Article:
Dedeoglu, S. orcid.org/0000-0001-7969-011X, Konstantopoulos, G. and Paspatis, A. (2021) Grid-supporting three-phase inverters with inherent RMS current limitation under balanced grid voltage sags. IEEE Transactions on Industrial Electronics, 68 (11). pp. 11379-11389. ISSN 0278-0046

https://doi.org/10.1109/TIE.2020.3034860

Grid-Supporting Three-Phase Inverters with Inherent RMS Current Limitation Under Balanced Grid Voltage Sags

Seyfullah Dedeoglu, *Student Member, IEEE*, George C. Konstantopoulos, *Member, IEEE*, and Alexandros G. Paspatis, *Member, IEEE*

***Abstract*—In this paper, a novel nonlinear droop control method is proposed for three-phase grid-supporting inverters that rigorously guarantees limited RMS value of the inverter current and closed-loop system stability under both normal grid conditions and balanced voltage sags. Contrary to the traditional *dq* frame approaches which align the inverter output voltage with the *d* axis, the proposed controller aligns the inverter current with the *d* axis resulting in the desired current limitation and detailed closed-loop system stability conditions. Inspired by the recently presented state-limiting PI controller and using nonlinear invariant set theory, it is rigorously proven that the RMS value of the inverter current is always limited below a given value, even during transients or faults, without requiring additional adaptive saturation units, as commonly applied in conventional approaches. Furthermore, analytic conditions for the controller parameter selection are provided to ensure asymptotic stability for the entire closed-loop grid supporting inverter for the first time without depending on particular values of the filter and line parameters. To verify the effectiveness of the proposed controller compared to existing current-limiting control methods, extensive simulation and experimental results of a three-phase inverter are provided under a normal grid and under different balanced voltage sag scenarios.**

***Index Terms*—Droop control, voltage sag, nonlinear control, RMS current limitation, stability analysis, three-phase inverter.**

I. Introduction

THE increasing integration of distributed energy resources (DERs) into the electricity grid, mainly through power inverter devices, is expected to significantly affect the grid strength and stability in the near future [1], [2]. Thus, more stringent requirements have been set by the grid operators that require inverter-interfaced DERs to provide ancillary services to the grid, by supporting the grid voltage and frequency [3], [4]. Since the desired operation of the inverter devices depends on their control mechanisms, advanced control schemes have been proposed for grid-connected inverter-based DER units to achieve a seamless integration and provide the necessary support under both normal and abnormal grid conditions, i.e. during grid faults [5]–[8].

The control operation of grid-supporting inverters is mainly based on the droop control concept which aims to contribute to the system stability, by regulating the grid voltage and frequency [7], [8]. Droop control is one of the most commonly used control methods for inverter-interfaced DERs, since it offers a communication-free operation, and mimics the working principle of the synchronous generators in terms of voltage and frequency regulation [9], [10]. Nevertheless, the required power measurements for the droop control operation introduce nonlinearities, which complicate the stability analysis of the closed-loop system [11]. Hence, when analytically assessing the closed-loop stability of a droop-controlled inverter, a root-locus analysis of the small-signal inverter model is widely considered [12]. However, root-locus analysis refers to a specific inverter application since it requires particular information on the inverter and filter parameters.

Furthermore, the stable and reliable operation of a grid-supporting inverter has to be guaranteed under both normal and abnormal grid conditions, especially during transients. When a sudden voltage sag occurs at the grid, the injected current by the inverter unit rapidly increases and can reach high values that can cause damage to the inverter device. To realize a current-limiting property, an adjustment of the reference inverter current is usually applied into the current-controlled inverters [5] and an adjustment of the reference powers (real and reactive) in inverters that follow low-voltage ride-through (LVRT) requirements is often employed. Nevertheless, the majority of these techniques ensure the desired current limitation only at the steady-state and not during the transient response [13], [14]. In grid-supporting inverters, the most common approach is the use of saturation units in the output of the inner-loop voltage controller [15], [16]. However, this approach causes a deactivation of the voltage controller during abnormal grid conditions, which can lead to integrator wind-up and instability [17], [18]. To address the issues mentioned above, a nonlinear current-limiting droop control technique, which does not utilize saturation units, thus avoiding the integrator wind-up, has been proposed in [19], [20] for single-phase grid-connected inverters and in [21] for three-phase rectifiers. However, this controller introduces additional integral states, which makes the hardware

Manuscript received May 20, 2020; revised July 23, 2020, and September 15, 2020; accepted October 11, 2020. This work is supported by EPSRC under Grants No EP/S001107/1 and EP/S031863/1.

The authors are with the Dept. of Automatic Control and Systems Engineering, The University of Sheffield, Sheffield, S1 3JD, UK. G. C. Konstantopoulos is with the Dept. of Electrical and Computer Engineering, University of Patras, Rion, 26500, Greece. E-mails: sdedeoglu1, g.konstantopoulos, apaspatis1@ sheffield.ac.uk.

implementation a difficult task. In the same framework, a nonlinear current-limiting controller is proposed in [22] using optimization techniques, but this scheme requires knowledge of the system parameters for the controller implementation and intensive computational effort. It should be highlighted that the majority of the current-limiting control approaches for three-phase inverters are designed on the synchronously rotating dq frame and aim to limit the d and $q-$axis of the inverter current separately [5], [12], [23]. Then, in order to ensure RMS current limitation, adaptive saturation units are utilised, which further complicate the implementation of the controller [24].

In this paper, a novel nonlinear control approach for three-phase grid-supporting inverters that inherently limits the RMS inverter current without the need of saturation units is proposed and analyzed. Inspired by the recently developed state-limiting PI controller in [25], the proposed controller is formulated to incorporate the widely used droop control concept and provide the necessary ancillary services to the grid. Then, using invariant set theory, it is rigorously proven for the first time that the proposed scheme ensures a desired limitation of the RMS inverter current below a given maximum value during the entire operation, i.e. during transients and at steady-state, irrespective of the grid conditions that might include grid faults (voltage sags). Opposed to the common droop control techniques, which align the inverter output voltage with the d axis [12], the novel idea of the proposed approach is based on the alignment of the local inverter current with the d axis using a suitable formulation of the inverter control input. The special structure of the proposed controller ensures that the desired RMS current limitation is maintained at all times, even during the transient response of a balanced grid voltage sag.

This idea was first proposed by the authors in [26], but implemented with a more complicated structure that included additional controller states. The main technical novelties and new contributions compared to [26] include: i) a new structure of the proposed controller which introduces less dynamic states, thus leading to a simplified implementation, ii) rigorous closed-loop system stability for the entire grid-supporting inverter without depending on the exact values of the inverter and filter parameters, iii) detailed comparison with conventional current-limiting control methods, and iv) extensive experimental results under a normal grid and under balanced voltage sags, to validate the proposed approach on a real setup.

Overall, compared to the existing droop control and current-limiting techniques, the proposed droop control approach for three-phase grid-supporting inverters inherits a desired RMS current limitation at all times, even during transients, without additional saturation units, while guaranteeing a stable closed-loop system. This is accomplished in a unified structure, without the need of modifying the controller during a grid voltage sag, as often required by LVRT methods, causing the RMS current to violate its desired maximum threshold during the transient [13], [14]. Furthermore, since no saturation units are required, contrary to conventional approaches [17], [18], the proposed method does not suffer from integrator windup, thus simplifying its implementation and facilitating the desired stability analysis. A thorough comparison with the conventional LVRT and current-limiting methods is presented in this paper to highlight the novelty of the proposed control approach, followed by an experimental validation.

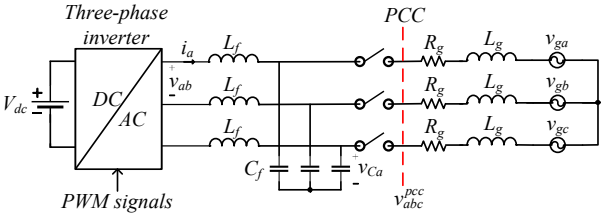

Fig. 1: Grid-connected three-phase inverter.

II. Dynamic System Modelling and Problem Definition

The system under consideration is a three-phase inverter which is connected to a point of common coupling (PCC) via an LC filter, as shown in Fig. 1. The filter inductance and capacitance are denoted as L_f, C_f, respectively, while the line resistance and inductance are expressed as R_g and L_g. Let v_{abc}^{pcc} be the balanced three phase voltages at the PCC, where V_{rms} and θ_g are the PCC RMS voltage and phase angle, respectively. Assuming the global dq frame PCC voltages are given as V_d^{pcc} and V_q^{pcc}, following the axis transformation in [26], the local dq frame PCC voltages are calculated as

$$\begin{bmatrix} V_{dl}^{pcc} \\ V_{ql}^{pcc} \end{bmatrix} = \begin{bmatrix} V_d^{pcc} cos\delta + V_q^{pcc} sin\delta \\ -V_d^{pcc} sin\delta + V_q^{pcc} cos\delta \end{bmatrix}. \tag{1}$$

where $\delta = \theta - \theta_g$ describes the phase angle difference between the inverter and the PCC. Thus, the dynamic equations of the three-phase inverter are given as

$$L_f \frac{di_d}{dt} = V_d + \omega L_f i_q - V_{dl}^{pcc} \tag{2}$$

$$L_f \frac{di_q}{dt} = V_q - \omega L_f i_d - V_{ql}^{pcc} \tag{3}$$

where i_d, i_q and V_d, V_q denote the dq frame local inverter currents and voltages, while $\omega = \dot{\theta}$ is the inverter angular frequency.

Considering the global PCC voltages V_d^{pcc}, V_q^{pcc} and the local currents, then the inverter active and reactive power can be computed as

$$\begin{aligned} P &= \tfrac{3}{2}\left[cos\delta\left(V_d^{pcc} i_d + V_q^{pcc} i_q\right) + sin\delta\left(V_q^{pcc} i_d - V_d^{pcc} i_q\right)\right] \\ Q &= \tfrac{3}{2}\left[cos\delta\left(V_q^{pcc} i_d - V_d^{pcc} i_q\right) - sin\delta\left(V_d^{pcc} i_d + V_q^{pcc} i_q\right)\right] \end{aligned} \tag{4}$$

To achieve the voltage and frequency regulation for grid support when required, the universal droop controller, with droop expressions $P \sim V$ and $Q \sim -\omega$, which can be applied independently of the inverter output impedance [10], will be used in this paper. Since the power expressions (4) are clearly nonlinear, the closed-loop system introduces nonlinear dynamics, which increase the difficulty in proving stability and ensuring a reliable and safe operation under both normal and faulty grid conditions. To this end, the main objective of this paper is to propose a novel control approach for implementing the droop functionality in three-phase grid-supporting inverters

that guarantees an RMS current limitation under both a normal grid and under balanced grid voltage sags, while rigorously ensuring closed-loop system stability.

III. Proposed Controller and Rms Current-Limiting Property

A. Proposed nonlinear controller

In order to ensure that the RMS value of the inverter current remains limited at all times, the proposed novel controller is based on the idea of orienting the inverter current to the local d axis, i.e. $i_q = 0$, and then implement a bounded dynamic controller that limits the d axis inverter current to a range of positive values and inherits the desired droop expression. In order to accomplish this task, the inverter voltage, which is the control input, is separated into two parts: a) a feed-forward term v_{abc}^{pcc} that contains the PCC voltage in the abc frame and b) a feedback control term $\bar{v}_{abc}$, obtained from a dq/abc transformation that implements the bounded nonlinear controller dynamics.

It should be underlined that the dynamic feedback term $\bar{v}_{abc}$ is disabled when the relay is open, i.e. when the PCC is disconnected, and enabled only when the relay is closed; hence the controller includes only the feed-forward term v_{abc}^{pcc} before connection, thus leading to a smooth grid connection and simultaneously avoiding the presence of circulating currents.

Hence, the proposed controller is introduced in the following scheme

$$v_{abc} = v_{abc}^{pcc} + \bar{v}_{abc} \tag{5}$$

where the feedback term $\bar{v}_{abc}$ is calculated from a dq/abc transformation using the angular frequency θ obtained considering the $Q \sim -\omega$ droop

$$\dot{\theta} = \omega = \omega^* + m\,(Q - Q_{set}) \tag{6}$$

where ω^* represents the rated grid angular frequency. Q_{set} is the reactive power reference and m indicates the reactive power droop coefficient. Consequently, the dq frame feedback term takes the form

$$\bar{v}_d = -r_v i_d + \frac{r_v I_{rms}^{max}}{\sqrt{2}}\,(1 + sin\sigma) - \omega L_f i_q \tag{7}$$

$$\bar{v}_q = -r_v i_q + \omega L_f i_d \tag{8}$$

where r_v is the constant virtual resistance, σ is the dynamic controller state, $\omega L_f i_d$ and $\omega L_f i_q$ are decoupling terms. In addition, I_{rms}^{max} is the maximum rated inverter RMS current which is defined by the user or the technical limitations of the inverter. Motivated by the recently proposed nonlinear state-limiting PI controller structure presented in [25], the dynamics for the controller state σ are given as

$$\dot{\sigma} = \frac{\sqrt{2}c}{r_v I_{rms}^{max}}\left[(E^* - V_{rms}) - n(P - P_{set})\right] cos\sigma \tag{9}$$

where c is the positive integral gain. By selecting the initial condition of σ to satisfy $\sigma_0 \in [-\frac{\pi}{2}, \frac{\pi}{2}]$, then it is guaranteed that $\sigma(t) \in [-\frac{\pi}{2}, \frac{\pi}{2}], \forall t \geq 0$. As it is explained in [25], the nonlinear dynamics have been carefully designed to avoid a continuously oscillating behavior of the controller state σ and additionally ensure that the controller dynamics slow down, i.e. $\dot{\sigma} \to 0$, as $\sigma \to \pm\frac{\pi}{2}$ (near the limits of the state σ), which illustrates an inherent integrator anti-windup property. Hence, the proposed controller does not result in any nonlinear phenomena that can lead to instability for the inverter system. Note that if initially σ_0 is selected as $\sigma_0 = -\frac{\pi}{2} + \epsilon$, for an arbitrarily small $\epsilon > 0$, then at the moment of the connection with the grid, since the inverter currents are very small before the connection, then both $\bar{v}_d$ and $\bar{v}_q$ will be very close to zero from (7)-(8), and a smooth transient can be achieved.

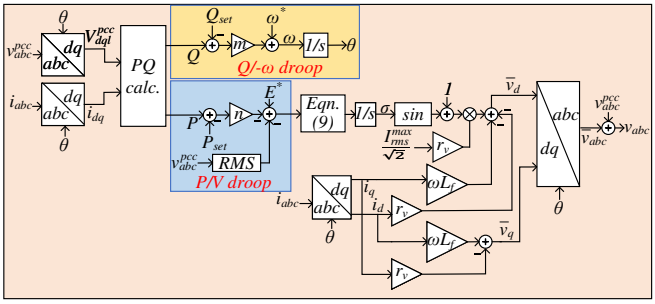

Fig. 2: Implementation diagram of the proposed controller.

Since the controller state σ represents an integral action, it leads to the regulation of the function $(E^* - V_{rms}) - n(P - P_{set})$, which describes the $P \sim V$ droop control that should be regulated to zero at the steady-state. In this droop function, E^* indicates the nominal RMS grid voltage, V_{rms} represents the RMS PCC voltage, which can be computed as $V_{rms} = \sqrt{\frac{(V_d^{pcc})^2 + (V_q^{pcc})^2}{2}}$, while P_{set} and n stand for the active power reference value and the active power droop coefficient, respectively. Note that by removing the term $(E^* - V_{rms})$ in (9), the controller can easily switch its operation from droop control to real power regulation. In order to illustrate the implementation of the proposed controller, a detailed diagram of its structure is provided in Fig. 2.

B. RMS current-limiting property

By implementing the controller dynamics (7) and (8) into the original inverter dynamics (2) and (3), the closed-loop inverter current equations can be written as

$$L_f \frac{di_d}{dt} = -r_v i_d + \frac{r_v I_{rms}^{max}}{\sqrt{2}}\,(1 + sin\sigma) \tag{10}$$

$$L_f \frac{di_q}{dt} = -r_v i_q \tag{11}$$

By defining $i_s = i_d - \frac{I_{rms}^{max}}{\sqrt{2}}$, then the equation (10) becomes

$$L_f \frac{di_s}{dt} = -r_v i_s + \frac{r_v I_{rms}^{max}}{\sqrt{2}} sin\sigma \tag{12}$$

where i_s is the shifted d axis current, which is defined to ensure the positiveness of the d axis current. This is necessary to ensure closed-loop asymptotic stability, as it will be explained in the next section. As it is clear from (11), the q axis current dynamics are independent providing the solution $(i_q(t) = i_q(0)e^{-\frac{r_v}{L_f}t})$, and therefore if initially $i_q(0) = 0$, then $i_q(t) = 0, \forall t \geq 0$. Thus, it is sufficient to prove that only the d axis current will be limited below a given maximum

value for guaranteeing the RMS current-limiting property at all times. Then, for system (12), the following continuously differentiable function can be considered:

$$V = \frac{1}{2} L_f i_s^2, \tag{13}$$

while its time derivative can be computed by utilizing (12) as

$$\begin{aligned} \dot{V} &= -r_v i_s^2 + \frac{r_v I_{rms}^{max}}{\sqrt{2}} i_s sin\sigma \\ &\leq -r_v i_s^2 + \frac{r_v I_{rms}^{max}}{\sqrt{2}} |i_s| \\ &\leq -r_v |i_s| (|i_s| - \frac{I_{rms}^{max}}{\sqrt{2}}). \end{aligned} \tag{14}$$

Hence, it becomes obvious from (14) that

$$\dot{V} < 0, \forall \mid i_s \mid > \frac{I_{rms}^{max}}{\sqrt{2}} \tag{15}$$

This means that the set $S = \{i_s \in R : |i_s| \leq \frac{I_{rms}^{max}}{\sqrt{2}}\}$ is invariant (since $\dot{V} \leq 0$ outside of S) [27], [28]. Hence, if initially $|i_s(0)| \leq \frac{I_{rms}^{max}}{\sqrt{2}}$, then

$$|i_s(t)| \leq \frac{I_{rms}^{max}}{\sqrt{2}}, \forall t \geq 0. \tag{16}$$

Since $i_s = i_d - \frac{I_{rms}^{max}}{\sqrt{2}}$, then (16) can be rewritten as

$$-\frac{I_{rms}^{max}}{\sqrt{2}} \leq i_d - \frac{I_{rms}^{max}}{\sqrt{2}} \leq \frac{I_{rms}^{max}}{\sqrt{2}}, \forall t \geq 0, \tag{17}$$

or equivalently

$$0 \leq i_d \leq \sqrt{2} I_{rms}^{max}, \forall t \geq 0. \tag{18}$$

Note, however, that by projecting the inverter current vector with amplitude $\sqrt{2} I_{rms}$, on the d and q axes, there is

$$\sqrt{i_d^2 + i_q^2} = \sqrt{2} I_{rms}. \tag{19}$$

Since $i_q = 0$, then $i_d = \sqrt{2} I_{rms}$ and consequently from (18), it is proven that

$$I_{rms} \leq I_{rms}^{max} \quad \forall t \geq 0, \tag{20}$$

which results in the desired RMS current-limiting property.

As can be understood from the analysis provided above, the current-limiting property is proven independently of the grid variables such as voltage, frequency, and angle, the droop functions, and the nonlinearities in the power expressions (4). Hence, this mathematical proof ensures a safe inverter operation under grid variations/faults or under unrealistic P_{set} values. In addition, contrary to [22], the proposed controller ensures that the system current will be limited at both transients and steady-state, and in contrast to [17], the integrator windup problem is inherently addressed using the state-limiting PI controller dynamics ($\dot{\sigma} \rightarrow 0$ when $\sigma \rightarrow \pm\frac{\pi}{2}$, or equivalently when $I_{rms} \rightarrow I_{rms}^{max}$) without the need for saturation blocks which might lead to system instability.

IV. Stability Analysis

In the previous section, it was proven that the RMS inverter current remains bounded below a given value regardless of the grid parameters or the active and reactive power set values. However, closed-loop system stability, in the sense of convergence to a desired equilibrium point, has not been guaranteed yet. Therefore, this section focuses on proving the asymptotic stability of the complete system. Taking into account that the power angle is given as $\delta = \theta - \theta_g$, then from (6) it yields

$$\dot{\delta} = \omega^* - \omega_g + m\left(Q - Q_{set}\right), \tag{21}$$

where ω_g is the PCC angular frequency. The closed-loop system dynamics are given now from (9)-(11) and (21). Without loss of generality, as done in [5], one can consider that $V_d^{pcc} = \sqrt{2} V_{rms}$ and $V_q^{pcc} = 0$ are constant (or equivalently close to the grid voltages at the global reference frame), and since it was proven in the previous section that the local q axis current of the inverter i_q remains at zero at all times, then the power expressions (4) can be simplified to

$$\begin{aligned} P &= \frac{3}{\sqrt{2}} V_{rms} i_d cos\delta \\ Q &= -\frac{3}{\sqrt{2}} V_{rms} i_d sin\delta. \end{aligned} \tag{22}$$

Considering (9)-(11), and (21), the closed-loop state vector becomes $x = [i_d \ \sigma \ \delta \ i_q]^T$. Let V_{rms} and ω_g take some constant (or piece-wise constant) values, not necessarily equal to their rated ones. Then the equilibrium point vector $x_e = [i_{de} \ \sigma_e \ \delta_e \ i_{qe}]^T$ can be calculated as

$$a)\ i_{de} = \frac{I_{rms}^{max}}{\sqrt{2}}(1 + sin\sigma_e) \tag{23}$$

$$b)\ \sigma_e = sin^{-1}\left(\frac{2}{3 V_{rms} cos\delta_e I_{rms}^{max}} \left(\frac{E^* - V_{rms}}{n} + P_{set}\right) - 1\right) \tag{24}$$

$$c)\ \delta_e = tan^{-1}\left(\frac{-\left(\frac{\omega_g - \omega^*}{m} + Q_{set}\right)}{\left(\frac{E^* - V_{rms}}{n} + P_{set}\right)}\right) \tag{25}$$

$$d)\ i_{qe} = 0 \tag{26}$$

where P_{set} and Q_{set} are active and reactive power set values, which can be changed by the control operator.

Now, the closed-loop system stability can be summarized in the following proposition.

Proposition 1. Every equilibrium point $x_e = [i_{de} \ \sigma_e \ \delta_e \ i_{qe}]^T$ of the closed-loop system (9)-(11), and (21), given by (23)-(26), with $\sigma_e, \delta_e \in (-\frac{\pi}{2}, \frac{\pi}{2})$, is asymptotically stable when r_v is chosen as

$$r_v > 3 m L_f V_{rms} I_{rms}^{max}, \tag{27}$$

and P_{set} and Q_{set} are selected to satisfy the inequality

$$\left| \frac{\omega^* - \omega_g}{m} - Q_{set} \right| \leq \left| \frac{E^* - V_{rms}}{n} + P_{set} \right|. \tag{28}$$

Proof: Given the equilibrium point $x_e = [i_{de}\ \sigma_e\ \delta_e\ i_{qe}]^T$, the Jacobian matrix of the closed-loop system takes the form,

$$J = \begin{bmatrix} J_T & 0_{3x1} \\ 0_{1x3} & -\frac{r_v}{L_f} \end{bmatrix}, \tag{29}$$

where

$$J_T = \begin{bmatrix} -\frac{r_v}{L_f} & \frac{r_v I_{rms}^{max} cos\sigma_e}{\sqrt{2}L_f} & 0 \\ -3\frac{V_{rms} cncos\sigma_e cos\delta_e}{r_v I_{rms}^{max}} & 0 & 3\frac{V_{rms} cni_{de} cos\sigma_e sin\delta_e}{r_v I_{rms}^{max}} \\ -\frac{3}{\sqrt{2}} m V_{rms} sin\delta_e & 0 & -\frac{3}{\sqrt{2}} m V_{rms} i_{de} cos\delta_e \end{bmatrix}. \tag{30}$$

Due to the block diagonal structure of matrix J in (29) and since $-\frac{r_v}{L_f}$ is negative, for the stability of the closed-loop system, it is only required to find the eigenvalues of J_T in (30). The characteristic equation of (30) can be formed as

$$\begin{aligned} &\lambda^3 + \left(\frac{3}{\sqrt{2}} m V_{rms} i_{de} cos\delta_e + \frac{r_v}{L_f}\right)\lambda^2 \\ &+ \left(\frac{3}{\sqrt{2}L_f} V_{rms} cos\delta_e \left(r_v m i_{de} + cncos^2\sigma_e\right)\right)\lambda \\ &+ \frac{9}{2L_f} cnm i_{de} cos^2\sigma_e V_{rms}^2 = 0 \end{aligned} \tag{31}$$

By applying the Routh-Hurwitz criterion, in order for all eigenvalues to have negative real parts, the following 3 stability conditions are obtained:

$$\left(\frac{3}{\sqrt{2}} m V_{rms} i_{de} cos\delta_e + \frac{r_v}{L_f}\right) > 0 \tag{32}$$

$$\frac{9}{2L_f} cnm i_{de} cos^2\sigma_e V_{rms}^2 > 0 \tag{33}$$

$$\frac{3}{\sqrt{2}L_f} V_{rms} cos\delta_e \left(r_v m i_{de} + cncos^2\sigma_e\right) > \frac{\frac{9}{2L_f} cnm i_{de} cos^2\sigma_e V_{rms}^2}{\left(\frac{3}{\sqrt{2}} m V_{rms} i_{de} cos\delta_e + \frac{r_v}{L_f}\right)}. \tag{34}$$

Since $\sigma_e \in (-\frac{\pi}{2}, \frac{\pi}{2})$, then from (23) there is $i_{de} > 0$, while from the current-limiting proof in the previous section, $i_{de} \leq \sqrt{2} I_{rms}^{max}$, i.e. $i_{de} \in (0, \sqrt{2} I_{rms}^{max}]$. As a result, condition (33) always holds. Note also that from (22) there is:

$$|P_e| = \left|\frac{3}{\sqrt{2}} V_{rms} i_{de} cos\delta_e\right| \leq 3 V_{rms} I_{rms}^{max}. \tag{35}$$

Given the selection of r_v according to (27) and taking into account (35), one can easily see that condition (32) is also satisfied.

Finally, condition (34) can be rewritten as

$$\begin{aligned} &\frac{3}{\sqrt{2}L_f} V_{rms} cos\delta_e \left(r_v m i_{de} + cncos^2\sigma_e\right)\left(\frac{3}{\sqrt{2}} m i_{de} V_{rms} cos\delta_e + \frac{r_v}{L_f}\right) \\ &- \frac{9}{2L_f} cnm i_{de} cos^2\sigma_e V_{rms}^2 > 0. \end{aligned} \tag{36}$$

By using the trigonometric property $cos^2\delta_e = 1 - sin^2\delta_e$, after some calculations, (36) results in

$$\begin{aligned} &\frac{9}{2L_f} V_{rms}^2 m^2 {i_{de}}^2 r_v + \frac{3}{\sqrt{2}L_f} V_{rms} \left(r_v m i_{de} + cncos^2\sigma_e\right) \cdot \\ &\frac{r_v cos\delta_e}{L_f} - \frac{3m}{\sqrt{2}} V_{rms} i_{de} sin^2\delta_e > 0. \end{aligned} \tag{37}$$

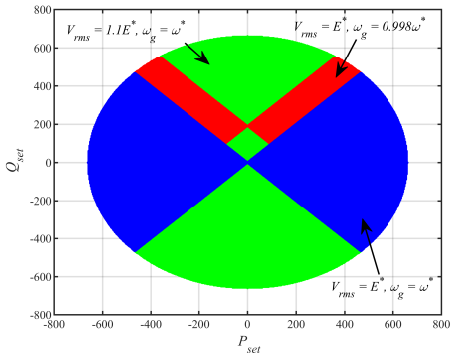

Fig. 3: Regions for selecting P_{set} and Q_{set} to ensure closed-loop stability.

In order for the above inequality to hold, it is sufficient to show that

$$\left(\frac{r_v cos\delta_e}{L_f} - \frac{3m}{\sqrt{2}} V_{rms} i_{de} sin^2\delta_e\right) \geq 0, \tag{38}$$

Now, by combining (27) and (35), it is guaranteed that

$$\frac{r_v}{L_f} > \frac{3}{\sqrt{2}} m V_{rms} i_{de} cos\delta_e. \tag{39}$$

Taking into account that $\delta_e \in (-\frac{\pi}{2}, \frac{\pi}{2})$, i.e., $0 < cos\delta_e \leq 1$, the following relation can be obtained

$$\frac{r_v}{L_f} cos\delta_e > \frac{3}{\sqrt{2}} m V_{rms} i_{de} cos^2\delta_e. \tag{40}$$

By combining (38) and (40), then to complete the stability analysis, it is sufficient to show that

$$\frac{3}{\sqrt{2}} m V_{rms} i_{de} (cos^2\delta_e - sin^2\delta_e) \geq 0. \tag{41}$$

Given that P_{set} and Q_{set} are selected according to (28), then from (25) it holds true that $-1 \leq tan\delta_e \leq 1$ which yields that $\delta_e \in [-\frac{\pi}{4}, \frac{\pi}{4}]$ or $\delta_e \in [\frac{3\pi}{4}, \frac{5\pi}{4}]$. Hence, it holds true that

$$cos^2\delta_e - sin^2\delta_e \geq 0, \tag{42}$$

which ensures that (41) is always satisfied. This completes the proof. ■

Remark 1. Proposition 1 provides a useful guidance for the selection of the controller parameter r_v. Note that if V_{rms} and L_f are not accurately known but vary within some given ranges, i.e. $V_{rms} \in [V_{rms}^{min}, V_{rms}^{max}]$ and $L_f \in [L_f^{min}, L_f^{max}]$, then r_v can be selected as

$$r_v > 3 m L_f^{max} V_{rms}^{max} I_{rms}^{max}, \tag{43}$$

which still satisfies (27). Similarly, the range for the values of P_{set} and Q_{set} can be calculated from (28), given that V_{rms} and ω_g can vary within some given ranges $V_{rms} \in [V_{rms}^{min}, V_{rms}^{max}]$ and $\omega_g \in [\omega_g^{min}, \omega_g^{max}]$.

Fig. 3 provides a guidance on how to select the values of P_{set} and Q_{set} for different values of V_{rms} and ω_g to ensure closed-loop system stability, taking as an example the parameters of Table II. In particular, in Fig. 3, it can be observed that with $V_{rms} = 1.1E^*$, the P_{set} and Q_{set} values can be selected anywhere within the green area, while for lower voltage and frequency values, the P_{set} and Q_{set} values

are restricted to the red or blue area. Note that these areas represent the sufficient conditions to ensure closed-loop system stability, i.e. the system may still be stable even if P_{set} and Q_{set} are selected outside of the provided ranges. However, these sets provide a useful guidance to the control operator to ensure stability is guaranteed at all times, based on the proof of Proposition 1.

It should be underlined that Proposition 1 guarantees closed-loop system stability for the inverter currents and the control dynamics. In order to prove closed-loop stability for the entire grid-connected inverter system, the dynamics of the remaining system, which include the capacitor voltages and grid side currents, should be investigated as well. These are given in the global dq frame as

$$C_f\frac{dV_{Cd}}{dt} = i_d cos\delta - i_q sin\delta + \omega_g C_f V_{Cq} - i_{gd} \tag{44}$$

$$C_f\frac{dV_{Cq}}{dt} = i_d sin\delta + i_q cos\delta - \omega_g C_f V_{Cd} - i_{gq} \tag{45}$$

$$L_g\frac{di_{gd}}{dt} = -R_g i_{gd} + \omega_g L_g i_{gq} + V_{Cd} - V_{gd} \tag{46}$$

$$L_g\frac{di_{gq}}{dt} = -R_g i_{gq} - \omega_g L_g i_{gd} + V_{Cq} - V_{gq} \tag{47}$$

where ω_g is the grid frequency and V_{dg}, V_{gq} are the dq-axis components of the grid voltage, which can be considered constant as in [5], to define the equilibrium point in (23)-(26). This system can be viewed as a linear-time invariant system and can be written in the standard form $\dot{x} = Ax + Bu$ with state vector $x = [V_{Cd}\ V_{Cq}\ i_{gd}\ i_{gq}]^T$ and input vector $u = [i_d cos\delta\ i_d sin\delta\ i_q cos\delta\ i_q sin\delta\ V_{gd}\ V_{gq}]^T$. Then, the A and B matrices can be constructed as

$$A = \begin{bmatrix} 0 & \omega_g & -\frac{1}{C_f} & 0 \\ -\omega_g & 0 & 0 & -\frac{1}{C_f} \\ \frac{1}{L_g} & 0 & -\frac{R_g}{L_g} & \omega_g \\ 0 & \frac{1}{L_g} & -\omega_g & -\frac{R_g}{L_g} \end{bmatrix}$$

$$B = \begin{bmatrix} \frac{1}{C_f} & 0 & 0 & -\frac{1}{C_f} & 0 & 0 \\ 0 & \frac{1}{C_f} & \frac{1}{C_f} & 0 & 0 & 0 \\ 0 & 0 & 0 & 0 & -\frac{1}{L_g} & 0 \\ 0 & 0 & 0 & 0 & 0 & -\frac{1}{L_g} \end{bmatrix}.$$

One can easily see that matrix A is Hurwitz independently of the filter, line and grid frequency parameters. Hence, system (44)-(47) is bounded-input bounded-state (BIBS) stable. Since the inverter currents (i_d, i_q) are proven to be bounded in Section III and the grid side voltages (V_{gd}, V_{gq}) are also bounded (constant or piecewise constant), then both the capacitor voltages V_{Cd}, V_{Cq} and the grid currents i_{gd}, i_{gq} are guaranteed to remain bounded at all times.

To complete the stability analysis of the entire closed-loop system, it should be proven that x converges to $x_e = [V_{Cde}\ V_{Cqe}\ i_{gde}\ i_{gqe}]^T$, which corresponds to $i_d = i_{de}$, $i_q = i_{qe}$ from (23)-(26) and constant V_{gd} and V_{gq} (not necessarily equal to their rated values). By setting $\tilde{x}_1 = x_1 - x_{1e} = [i_d\ \sigma\ \delta\ i_q]^T - [i_{de}\ \sigma_e\ \delta_e\ i_{qe}]^T$ and $\tilde{x}_2 = x_2 - x_{2e} = [V_{Cd}\ V_{Cq}\ i_{gd}\ i_{gq}]^T - [V_{Cde}\ V_{Cqe}\ i_{gde}\ i_{gqe}]^T$, then the entire closed-loop system given from (9)-(11), (21), (44)-(47) can be written in the form of two interconnected systems as

$$\dot{\tilde{x}}_1 = f(\tilde{x}_1) \tag{48}$$

$$\dot{\tilde{x}}_2 = g(\tilde{x}_1, \tilde{x}_2). \tag{49}$$

Based on Proposition 1, system (9)-(11), (21) is asymptotically stable at $[i_{de}\ \sigma_e\ \delta_e\ i_{qe}]^T$, then equivalently (48) is asymptotically stable at the origin. In the same framework, since the linear system (44)-(47) is BIBS with respect to the input u, and V_{gd}, V_{gq} are constant, then consequently (49) is BIBS with respect to $\tilde{x}_1$. Then, according to Lemma 5.6 in [27], it is proven that the interconnected system (48)-(49) is also asymptotically stable at the origin, yielding that the remaining system states $[V_{Cd}\ V_{Cq}\ i_{gd}\ i_{gq}]^T$ asymptotically converge to $[V_{Cde}\ V_{Cqe}\ i_{gde}\ i_{gqe}]^T$. This completes the stability analysis of the entire closed-loop system.

TABLE I: System and Controller Parameters for Comparison Studies

Parameters	Values	Parameters	Values
Power System Parameters			
L_f	$2.2mH$	L_g	$0.028mH$
R_f	0.5Ω	R_g	0.04Ω
ω^*	$2\pi 50\ rad/s$	I_{rms}^{max}	$20A$
S	13200VA	V_{dc}	$800V$
E^*	$220V$	C_f	$1\mu F$
Proposed Controller Parameters			
n	0.0017	m	0.0012
r_v	20Ω	c	3000
Saturation and LVRT Controller Parameters			
k_{pi}, k_{ii}	$4,200$	k_{pv}, k_{iv}	$0.03, 1.2$
n	0.0047	m	0.0012
r_v	0.7Ω	k_{pfrt}, k_{ifrt}	$0.04, 2.5$

V. Performance Comparison with Conventional Control Methods

In order to evaluate the proposed controller performance and highlight the novel contribution compared to other recently proposed methods, in this section, comparative simulation results are presented using the Matlab/Simulink environment. In particular, the proposed control scheme is compared with two widely used current-limiting methods for inverter-interfaced DERs. Both benchmark schemes are based on the cascaded droop control scheme presented in [12], while adopting the $P \sim V$ and $Q \sim -\omega$ droop relations proposed in [14] to have a direct comparison. The simulation parameters are shown in Table I. Regarding the conventional current-limiting methods, the first benchmark scheme (Benchmark Ctrl 1) uses saturation units at the output of the voltage controller, as explained in [17], while the second method (Benchmark Ctrl 2) follows an LVRT technique to limit the injected power (thus limiting the inverter current as well), as in [13], [14].

Initially, the proposed controller is compared with the Benchmark Ctrl 1, with the performed scenario being as follows: At the beginning, the inverter is not connected to the grid, since the relay is open. At $t = 0.2s$, the relay closes and the inverter is connected to the grid, with P_{set} and Q_{set} having initially the values of $4000\,\mathrm{W}$ and $0\,\mathrm{Var}$, while they are changed to $8000\,\mathrm{W}$ and $2000\,\mathrm{Var}$ at $t = 0.5s$ and $t = 1s$, respectively. As it is depicted in Fig. 4a and Fig. 4c, both the Benchmark Ctrl 1 and the proposed controller regulate their

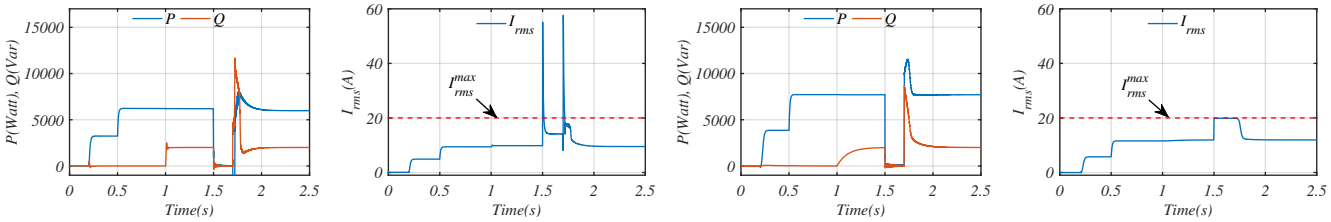

Fig. 4: Performance comparison between the Benchmark Ctrl 1 (a)-(b) and the Proposed controller (c)-(d) under a three-phase short circuit fault.

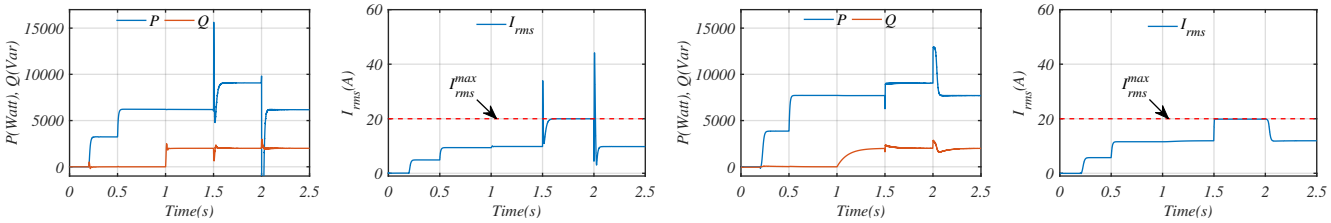

Fig. 5: Performance comparison between the Benchmark Ctrl 2 (a)-(b) and the Proposed controller (c)-(d) under a 30% balanced grid voltage sag.

output powers to the desired values according to droop control. From the same figure, it can be understood that the operation of the inverter under the two control schemes is similar under normal grid conditions. However, at $t = 1.5s$, a bolted short circuit occurs at the grid voltage and last for $0.2s$. During this fault, it can be seen in Fig. 4b that the Benchmark Ctrl 1 fails to limit the inverter current during the fault appearance and clearance transients, while during the steady state, the maximum available power is not utilized, since the d and q axis inverter currents are limited independently to ensure in the worst case that $I_{rms} \leq I_{rms}^{max}$. In contrast, the proposed controller effectively limits the inverter current during both the transient and the steady-state as shown in Fig. 4d, while the inverter current is maximized during the fault to provide maximum voltage support.

Next, the proposed controller is compared to the Benchmark Ctrl 2. While the normal grid operation is the same with the previous comparison as shown in Fig. 5a and Fig. 5c, here a balanced 30% voltage drop is applied at the grid voltage at $t = 1.5s$ and lasts for $0.5s$. It is highlighted in Fig. 5b that even if the LVRT limitation technique of the Benchmark Ctrl 2 manages to provide maximum voltage support during the fault, the maximum inverter current threshold is again violated during the fault appearance and clearance transients. On the other hand, using the proposed controller in the same faulty conditions, the current is again safely regulated to its maximum value as shown in Fig. 5d. Hence, as it is illustrated in the presented simulation study, the proposed controller outperforms the benchmark control schemes, in terms of its transient current-limiting property and the maximization of the injected power during balanced grid faults.

VI. Experimental Verification

In order to further validate the effectiveness of the proposed controller, a 660 VA three-phase grid-connected inverter was

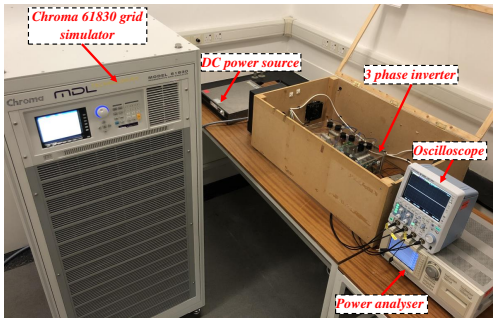

Fig. 6: Experimental setup.

TABLE II: Experiment and control parameters

Parameters	Values	Parameters	Values
L_f	$5.7mH$	L_g	$4.4mH$
R_g	0.5Ω	C_f	$1\mu F$
ω^*	$2\pi 50\ rad/s$	I_{rms}^{max}	$2A$
n	0.0117	m	0.0033
S	660VA	V_{dc}	$350V$
E^*	$110V$	f_{sw}	$16kHz$
r_v	20Ω	c	50

experimentally tested. The inverter was connected to a Chroma 61830 grid simulator via an LC filter and a line, as shown in Fig. 6. The controller was implemented as in Fig. 2 using a dSPACE 1104 control card with a sampling frequency of 15 kHz, while the system and controller parameters are given in Table II. The droop coefficients were chosen as in [10], [19].

A. Normal grid operation

Initially, normal grid conditions are considered and in Fig. 7a, the following scenario is performed. At $t_1 = 0.6s$, the inverter is connected to the grid, with the real power regulation mode is initially enabled and the real and reactive power reference values being 300 W and 0 Var, respectively. At $t_2 = 6.6s$, the real power reference value is increased to 500 W and at $t_3 = 12.6s$, the reactive power reference is

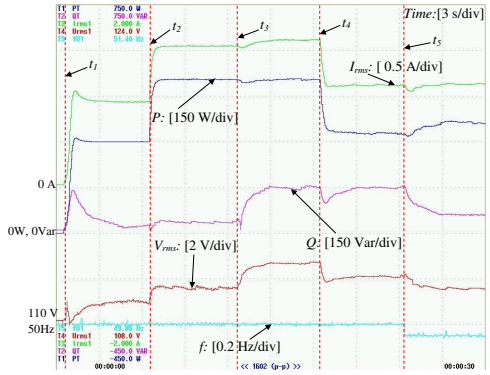

(a) Time response of P, Q, I_{rms}, V_{rms} and f

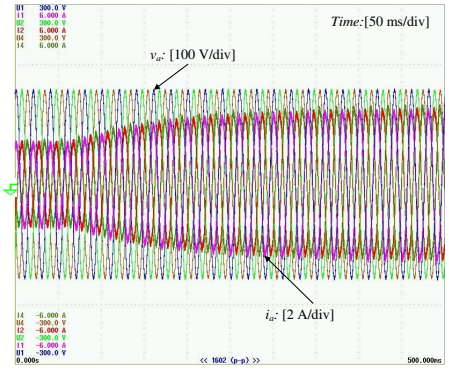

(b) Current transient when P_{set} is increased from $300\,W$ to $750\,W$

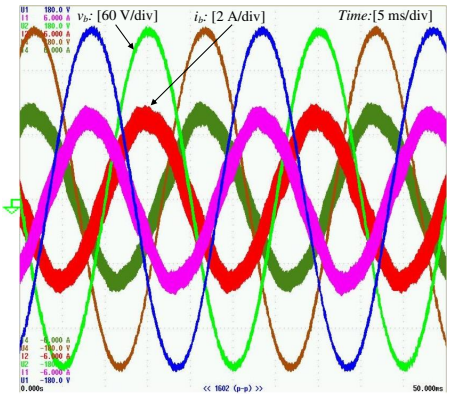

(c) Steady-state inverter voltages and currents

Fig. 7: Grid-supporting inverter operation under the proposed controller during normal grid conditions.

changed to 150 Var. As it can be seen in Fig. 7a, the proposed controller quickly regulates P and Q to their desired reference values. Note that small inaccuracies are present at the reactive power measurement near the zero value due to limitations of the power analyser in low values (near zero). To verify the droop control operation, the active power droop is enabled at $t_4 = 18.4s$ and P is quickly regulated at its new steady-state value, which can be calculated as $\frac{E^* - V_{rms}}{n} + P_{set}$ from (9), to regulate the inverter output voltage closer to its rated value. Likewise, to verify the reactive power droop control operation, a drop from 50 Hz to 49.95 Hz is applied to the grid frequency using the grid simulator, at $t_5 = 24.3s$. Thus, the reactive power drops in accordance to the frequency difference with respect to its nominal value. In order to validate the current-limiting property of the proposed controller, at $t = 75ms$ in Fig. 7b, the active power reference is increased from 300 W to 750 W with reactive power reference value being 0 Var, which represents a demand higher than the maximum apparent power of the inverter. However, as shown in Fig. 7b and proven in the theoretic part of this paper, I_{rms} is limited to 1.84 A, thus limiting the real power to 607.2 W, which is slightly below the maximum inverter apparent power. It is underlined that the RMS inverter current is limited to a slightly lower value than I_{rms}^{max} because in the theoretic design of the controller, the parasitic resistance of the filter inductor was neglected. In fact, if the filter inductor L_f introduces a small series resistance r_f, then from the resulting closed-loop inverter current dynamics at the steady-state, given similarly to (10), one can calculate the maximum steady-state RMS value of the current as $I_{rmse}^{max} = \frac{r_v}{r_f + r_v} I_{rms}^{max}$. In order to fully utilise the inverter current-limiting capability, the virtual resistor r_v can be selected to dominate the parasitic resistance r_f (i.e. $r_v >> r_f$) or the d-axis dynamic feedback term (7) can be modified as

$$\bar{v}_d = -r_v i_d + \frac{(r_f + r_v) I_{rms}^{max}}{\sqrt{2}} (1 + sin\sigma) - \omega L_f i_q \qquad (50)$$

Note that this modification does not affect the theoretical proof provided above and $I_{rms} < I_{rms}^{max}$ will still hold, which is required for the safe inverter operation. However, even with the proposed control design, which does not require knowledge of this parasitic resistance, the RMS current is limited below the maximum value as desired, offering a more robust controller implementation.

Furthermore, Fig. 7c shows the steady-state inverter current and voltage measurements when I_{rms} has reached I_{rms}^{max}. The visible ripples in the current waveforms are expected as these represent the inverter-side currents. In fact, a 10% THD has been calculated for these waveforms using the Yokogawa WT1800 power analyser. Nevertheless, since the THD of the grid-side currents is more important for a grid-connected inverter case, this has been calculated as 4.5%, which falls within the acceptable range according to the IEEE 519-2014 standard for low grid voltage applications [29], [30]. A further reduction of the THD can be achieved if inner current control loops are adopted or a different filter is selected. It is underlined that even if a different filter is selected, the RMS current-limiting property and the stability analysis presented in this paper are still valid, as they do not depend on the particular values of the filter parameters L_f, C_f or L_g. However, in the case where inner current control loops are added to the controller implementation, further investigation is required for the stability analysis of the entire system. Nevertheless, the purpose of this work is to propose for the first time this novel control structure and simultaneously guarantee the stability in a rigorous manner. Thus, it has been verified that the proposed controller supports the grid via the desired droop control operation and additionally offers an inherent protection of the inverter against excessive power demands.

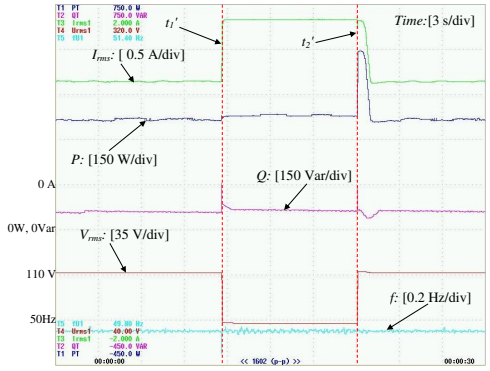

(a) Time response of P, Q, I_{rms}, V_{rms} and f

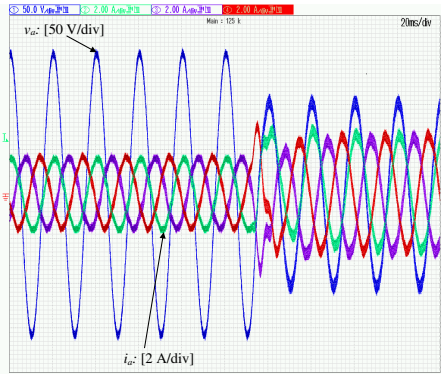

(b) Inverter currents and PCC phase-a voltage when the fault occurs

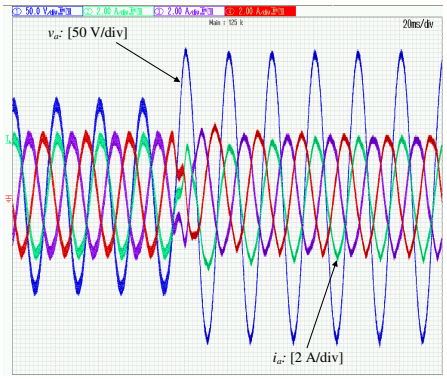

(c) Inverter currents and PCC phase-a voltage when the fault is cleared

Fig. 8: Grid-supporting inverter response under the proposed controller when a balanced voltage sag $110\,V \rightarrow 70\,V$ occurs.

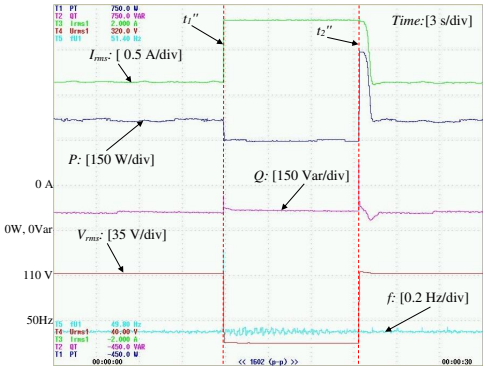

(a) Time response of P, Q, I_{rms}, V_{rms} and f

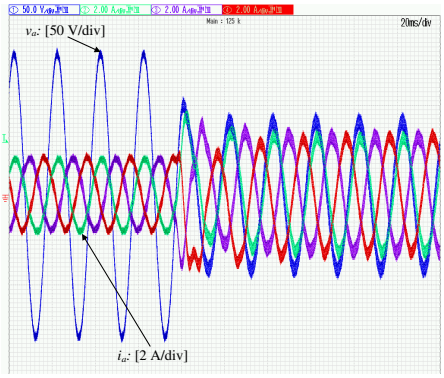

(b) Inverter currents and PCC phase-a voltage when the fault occurs

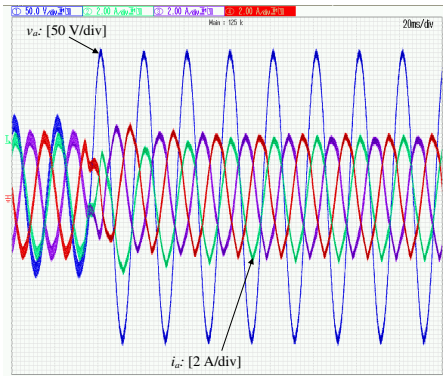

(c) Inverter currents and PCC phase-a voltage when the fault is cleared

Fig. 9: Grid-supporting inverter response under the proposed controller when a balanced voltage sag $110\,V \rightarrow 55\,V$ occurs.

B. Operation under balanced grid voltage sags

To further validate the performance of the proposed control scheme, grid fault cases in terms of balanced voltage sags are examined in this section, while the inverter is operating in the desired droop control mode.

Initially, the grid voltage drops from $110\,\mathrm{V}$ to $70\,\mathrm{V}$ at $t_1^{'} = 11.6s$ in Fig. 8a. During the fault, the RMS value of the current increases to its maximum value without violating the desired upper threshold. Hence, the proposed controller maximizes the power injection, while inherently protecting the inverter device. This operation can be theoretically explained as follows: when the fault appears, the controller state σ converges to its maximum value, which is $\frac{\pi}{2}$. In that case, the integration (9) tends to zero due to the cosine term in the dynamics, and therefore, acts like an inherent integrator anti-windup technique. As it is clear in Fig. 8a, when the current is limited at $1.85\,\mathrm{A}$, P increases to $384.6\,\mathrm{W}$, which can be calculated as $(\sqrt{S^2 - Q^2} = \sqrt{(3 \times 1.85 \times 70)^2 - 55^2})$. When the fault is cleared at $t_2^{'} = 21s$, the real and reactive powers return to their original values, according to the droop control. In Fig. 8b and Fig. 8c, the transient response of the inverter current and the PCC voltage are depicted during the fault appearance and the fault clearance. It is underlined that due to the limited number of the channels available in the oscilloscope (4 in total), only one voltage (phase a) and three

current measurements are shown in the Figures 8b, 8c, 9b, and 9c. Since the paper examines balanced voltage sags, the other phases (b and c) of the grid voltage follow the same drop ratio as phase a. As it is clear, the RMS value of the inverter current never violates its maximum value, as desired.

In order to test the controller performance under larger grid voltage sags, experimental results where the grid voltage drops from $110\,\mathrm{V}$ to $55\,\mathrm{V}$ are provided in Fig 9a. When the fault appears at $t_1^{''} = 11.9s$, I_{rms} increases again to $1.85\,\mathrm{A}$ (i.e. very close to I_{rms}^{max}), while the reactive power remains at its steady-state value. Hence, the real power during this voltage drop can be calculated as $300\,\mathrm{W}$ ($\sqrt{S^2 - Q^2} = \sqrt{(3 \times 1.85 \times 55)^2 - 55^2}$), as depicted in Fig. 9a. When the fault is cleared at $t_2^{''} = 21.3s$, the real and reactive powers return to their former values, after a short transient. Fault appearance and clearance under the 50% grid voltage drop can be observed in detail in Fig. 9b and Fig. 9c. As a result, the desired grid support capability of the inverter and its inherent RMS current-limiting property have been confirmed under both normal and faulty grid conditions that include balanced voltage sags verifying the theoretic contribution and the stability analysis presented in this work.

VII. Conclusion

A novel nonlinear current-limiting droop controller for three-phase grid-connected inverters has been introduced in this paper. The limitation of the RMS value of the inverter current was guaranteed for the first time without requiring adaptive saturation units through a rigorous analysis based on invariant set theory, under both a normal grid and under balanced voltage sags. A detailed proof of the closed-loop asymptotic system stability was presented without requiring full knowledge of the inverter filter parameters, which also provides a useful guidance on the selection of the controller parameters for the control implementation. To emphasize the superiority of the proposed controller over existing current-limiting methods, extensive comparison studies have been realized. The theoretic contributions of the paper and the effectiveness of the proposed control scheme were confirmed using an experimental setup consisting of a three-phase grid-connected inverter operating under a normal grid and under different levels of balanced voltage sags.

Future work will focus on the investigation of the proposed current-limiting control scheme in different faulty grid scenarios that include short circuits of line-to-ground and line-to-line (with and without ground), with the inclusion of a rigorous stability analysis for every individual case. Furthermore, inner current loops will be added to the controller implementation in order to further decrease the grid current THD and the stability of the complete system that includes the additional control loops will be examined.

References

[1] G. G. Talapur, H. M. Suryawanshi, L. Xu and A. B. Shitole, "A Reliable Microgrid With Seamless Transition Between Grid Connected and Islanded Mode for Residential Community With Enhanced Power Quality," *IEEE Trans. Ind. Appl.*, vol. 54, no. 5, pp. 5246-5255, Sept.-Oct. 2018.

[2] B. Kroposki et al., "Achieving a 100% Renewable Grid: Operating Electric Power Systems with Extremely High Levels of Variable Renewable Energy," *IEEE Power Energy Mag.*, vol. 15, no. 2, pp. 61-73, March-April 2017.

[3] H. Farhangi, "The path of the smart grid," *IEEE Power Energy Mag.*, vol. 8, no. 1, pp. 18-28, January-February 2010.

[4] J. Rocabert, A. Luna, F. Blaabjerg and P. Rodríguez, "Control of Power Converters in AC Microgrids," *IEEE Trans. Power Electron.*, vol. 27, no. 11, pp. 4734-4749, Nov. 2012.

[5] L. Huang et al., "A Virtual Synchronous Control for Voltage-Source Converters Utilizing Dynamics of DC-Link Capacitor to Realize Self-Synchronization," *IEEE J. Emerg. Sel. Top. Power Electron.*, vol. 5, no. 4, pp. 1565-1577, Dec. 2017, doi: 10.1109/JESTPE.2017.2740424.

[6] Y. Levron, J. Belikov, and D. Baimel, "A Tutorial on Dynamics and Control of Power Systems with Distributed and Renewable Energy Sources Based on the DQ0 Transformation," *Appl. Sci.*, vol. 8, no. 9, p. 1661, 2018, doi: 10.3390/app8091661.

[7] X. Meng, J. Liu and Z. Liu, "A Generalized Droop Control for Grid-Supporting Inverter Based on Comparison Between Traditional Droop Control and Virtual Synchronous Generator Control," *IEEE Trans. Power Electron.*, vol. 34, no. 6, pp. 5416-5438, June 2019.

[8] S. A. Khajehoddin, M. Karimi-Ghartemani and M. Ebrahimi, "Grid-Supporting Inverters With Improved Dynamics," *IEEE Trans. Ind. Electron.*, vol. 66, no. 5, pp. 3655-3667, May 2019.

[9] J. M. Guerrero, J. Matas, L. Garcia de Vicuna, M. Castilla and J. Miret, "Decentralized Control for Parallel Operation of Distributed Generation Inverters Using Resistive Output Impedance," *IEEE Trans. Ind. Electron.*, vol. 54, no. 2, pp. 994-1004, April 2007.

[10] Q. Zhong and Y. Zeng, "Universal Droop Control of Inverters With Different Types of Output Impedance," *IEEE Access*, vol. 4, pp. 702-712, 2016.

[11] J. W. Simpson-Porco, F. Dörfler and F. Bullo, "Voltage Stabilization in Microgrids via Quadratic Droop Control," *IEEE Trans. Automat. Contr.*, vol. 62, no. 3, pp. 1239-1253, March 2017, doi: 10.1109/TAC.2016.2585094.

[12] N. Pogaku, M. Prodanovic and T. C. Green, "Modeling, Analysis and Testing of Autonomous Operation of an Inverter-Based Microgrid," *IEEE Trans. Power Electron.*, vol. 22, no. 2, pp. 613-625, March 2007, doi: 10.1109/TPEL.2006.890003.

[13] P. Piya, M. Ebrahimi, M. Karimi-Ghartemani and S. A. Khajehoddin, "Fault Ride-Through Capability of Voltage-Controlled Inverters," *IEEE Trans. Ind. Electron.*, vol. 65, no. 10, pp. 7933-7943, Oct. 2018, doi: 10.1109/TIE.2018.2803765.

[14] X. Zhao, J. M. Guerrero, M. Savaghebi, J. C. Vasquez, X. Wu and K. Sun, "Low-Voltage Ride-Through Operation of Power Converters in Grid-Interactive Microgrids by Using Negative-Sequence Droop Control," *IEEE Trans. Power Electron.*, vol. 32, no. 4, pp. 3128-3142, April 2017, doi: 10.1109/TPEL.2016.2570204.

[15] Y. Yang, F. Blaabjerg and H. Wang, "Low-Voltage Ride-Through of Single-Phase Transformerless Photovoltaic Inverters," *IEEE Trans. Ind. Appl.*, vol. 50, no. 3, pp. 1942-1952, May-June 2014.

[16] M. S. El Moursi, W. Xiao and J. L. Kirtley, "Fault ride through capability for grid interfacing large scale PV power plants," *IET Gener. Transm. Distrib.*, vol. 7, no. 9, pp. 1027-1036, Sept. 2013.

[17] N. Bottrell and T. C. Green, "Comparison of Current-Limiting Strategies During Fault Ride-Through of Inverters to Prevent Latch-Up and Wind-Up," *IEEE Trans. Power Electron.*, vol. 29, no. 7, pp. 3786-3797, July 2014.

[18] A. D. Paquette and D. M. Divan, "Virtual Impedance Current Limiting for Inverters in Microgrids With Synchronous Generators," *IEEE Trans. Ind. Appl.*, vol. 51, no. 2, pp. 1630-1638, March-April 2015.

[19] Q. Zhong and G. C. Konstantopoulos, "Current-Limiting Droop Control of Grid-Connected Inverters," *IEEE Trans. Ind. Electron.*, vol. 64, no. 7, pp. 5963-5973, July 2017.

[20] G. C. Konstantopoulos, Q. Zhong and W. Ming, "PLL-Less Nonlinear Current-Limiting Controller for Single-Phase Grid-Tied Inverters: Design, Stability Analysis, and Operation Under Grid Faults," *IEEE Trans. Ind. Electron.*, vol. 63, no. 9, pp. 5582-5591, Sept. 2016

[21] Q. Zhong and G. C. Konstantopoulos, "Current-Limiting Three-Phase Rectifiers," *IEEE Trans. Ind. Electron.*, vol. 65, no. 2, pp. 957-967, Feb. 2018.

[22] D. Groß and F. Dörfler, "Projected grid-forming control for current-limiting of power converters," in *57Th Annu. Allert. Conf. Commun. Control. Comput.*, 2019, pp. 326-333.

[23] X. Tang, W. Deng and Z. Qi, "Investigation of the Dynamic Stability of Microgrid," *IEEE Trans. Power Syst.*, vol. 29, no. 2, pp. 698-706, March 2014.

[24] S. Acharya, M. S. El-Moursi, A. Al-Hinai, A. S. Al-Sumaiti and H. H. Zeineldin, "A Control Strategy for Voltage Unbalance Mitigation in an Islanded Microgrid Considering Demand Side Management Capability," *IEEE Trans. Smart Grid*, 2019, pp. 2558-2568.
[25] G. C. Konstantopoulos and P. R. Baldivieso-Monasterios, "State-limiting PID controller for a class of nonlinear systems with constant uncertainties," *Int. J. Robust Nonlinear Control*, vol. 30, no. 5, pp. 1770-1787, 2020, doi: 10.1002/rnc.4853.
[26] S. Dedeoglu and G. C. Konstantopoulos, "PLL-Less Three-Phase Droop-Controlled Inverter with Inherent Current-Limiting Property," in *45th Annu. Conf. of the IEEE Ind. Electron. Soc.*, 2019, pp. 4013-4018.
[27] H. K. Khalil, *Nonlinear Systems*, Prentice Hall: Upper Saddle River, NJ, USA, 1996.
[28] A. T. Alexandridis, "Studying State Convergence of Input-to-State Stable Systems with Applications to Power System Analysis," *Energies*, vol. 13, no. 1, p. 92, Dec. 2019.
[29] IEEE Recommended Practice and Requirements for Harmonic Control in Electric Power Systems," *IEEE Std 519-2014 (Revision of IEEE Std 519-1992)*, vol., no., pp.1-29, 11 June 2014, doi: 10.1109/IEEESTD.2014.6826459.
[30] M. Liserre, F. Blaabjerg and S. Hansen, "Design and control of an LCL-filter-based three-phase active rectifier," *IEEE Trans. Ind. Appl.*, vol. 41, no. 5, pp. 1281-1291, Sept.-Oct. 2005, doi: 10.1109/TIA.2005.853373.

Seyfullah Dedeoglu (S'17) received his Diploma degree from the Department of Electrical and Electronics Engineering, Sakarya University, Sakarya, Turkey, in 2014, and Master degree from the Department of Automatic Control and Systems Engineering, The University of Sheffield, Sheffield, UK, in 2017, where he is currently working towards the Ph.D. degree. In 2015, he got a scholarship that fully covers his Master and PhD education from the Ministry of National Education of Turkey. His current research interests include nonlinear control and stability analysis of unidirectional and bidirectional power converters in renewable energy and smart grid applications.

George C. Konstantopoulos (S'07-M'13) received his Dipl.Eng. and Ph.D. degrees in electrical and computer engineering from the Department of Electrical and Computer Engineering, University of Patras, Rion, Greece, in 2008 and 2012, respectively. From 2011 to 2012, he was an Electrical Engineer with the Public Power Corporation of Greece. Since 2013, he has been with the Department of Automatic Control and Systems Engineering, The University of Sheffield, U.K., holding the positions of Research Associate, Research Fellow, Lecturer and Senior Lecturer. Since 2019, he has been with the Department of Electrical and Computer Engineering, University of Patras, Greece, as an Associate Professor. He is an EPSRC UKRI Innovation Fellow in the priority area of cheap and clean energy technologies and he currently serves as an Associate Editor of the IET Smart Grid Journal and the International Journal of Systems Science. His research interests include nonlinear modeling, control and stability analysis of power converters in microgrid and smart grid applications, renewable energy systems and electrical drives. Dr. Konstantopoulos is a Member of the National Technical Chamber of Greece.

Alexandros G. Paspatis (S'12-M'21) received the Diploma in Electrical and Computer Engineering from the Democritus University of Thrace, Greece, in 2016 and the Ph.D. degree from The University of Sheffield, UK, in 2020. During 2018, he was a Research Assistant in the Department of Automatic Control and Systems Engineering, The University of Sheffield, UK. Since 2020, he has been with the Department of Electrical and Computer Engineering, Hellenic Mediterranean University, Greece, as a Postdoctoral Researcher. His research interests lie in analysis, control and stability of inverter-dominated power systems. He is a Member of the Technical Chamber of Greece.